Hydration of lime-marine sediment blends: Influence of mineralogical composition and lime content

Salim Kourtaa, Morgan Chabannes, Frédéric Becquart, Nor-Edine Abriak

Hydration of lime—marine sediment blends: influence of mineralogical composition and lime content

Salim Kourtaa[1,2], Morgan Chabannes[1,2,*], Frédéric Becquart[1,2], Nor-Edine Abriak[1,2]

[1]IMT Nord Europe, Institut Mines-Télécom, Centre for Materials and Processes, F-59000 Lille, France
[2]Univ. Lille, Institut Mines-Télécom, ULR 4515 – LGCgE, Laboratoire de Génie Civil et géo-Environnement, F-59000 Lille, France

*Corresponding author: morgan.chabannes@imt-nord-europe.fr

Abstract

There is a need to find alternatives to the extraction of non-renewable mineral resources for the production of new binders. Some specific building materials such as plant-aggregate-based concretes do not require high-strength binders. In this context, the lime-pozzolan technology, inherited from Roman times, can help reduce the carbon footprint of finished materials by the use of low amounts of lime. In this paper, three different marine dredged sediments were used as natural alumino-silicate resources and blended with hydrated lime. Based on previous literature dealing with the pozzolanic activity of cristallized minerals, the sediments were reduced to micronized powders. The hydration of these systems was investigated through hardening and reaction kinetics up to 365 days at 20°C and 50°C. The sediments used revealed two kinds of mineral assemblages and the best pozzolanic reactivity was found with quartz-rich sediments. In addition, the optimum lime content was found to be 20 wt% until 180 days.

Key-words: Marine sediments; micronized powders; mineralogy; lime content; low-carbon binders

Graphical Abstract

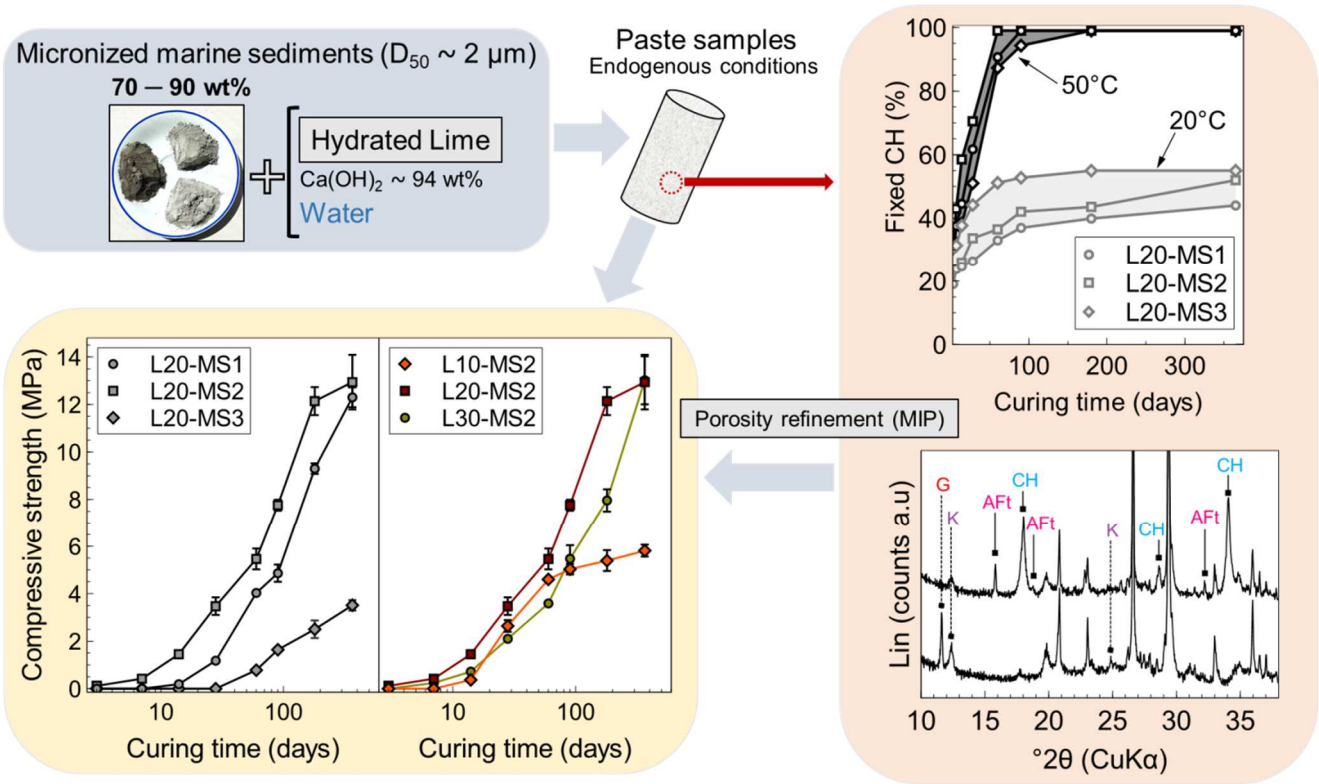

1. Introduction

Reducing carbon emissions in buildings is a critical issue for which the use of bio-based materials can make a real contribution. Based upon old building methods, hemp concrete has been the subject of many research works since the beginning of the 1990s, especially in Northern Europe [1]. To produce hemp concrete, plant-derived aggregates (hemp shives) are mixed with lime-based binders (mix of hydrated lime with hydraulic binders). The carbon emissions due to the production of these binders is reported to heavily contribute to the Global Warming Potential (GWP) in many studies dealing with Life Cycle Assessment (LCA) of hemp concretes [2,3,4].

In Roman times, significant advances were made in lime technology by adding reactive alumino-silicate materials such as volcanic ashes (i.e. natural pozzolans) or particles of crushed bricks, thus providing hydraulic properties to the binders [5,6]. Since the development of Portland cement in the beginning of the 19th century, lime-pozzolan binders have become marginal whereas their use for specific applications (building refurbishment, low-carbon construction) is still of interest. Realizing that carbon emissions are primarily due to the decarbonation of limestone for the production of lime, the use of materials with pozzolanic properties definitely appears to be a relevant opportunity to include only low amounts of lime into the binder [7], thereby reducing the carbon footprint of bio-based materials like hemp concrete. According to ASTM C125-07 standard, a pozzolan is defined as a siliceous or silico-aluminous material able to combine lime at ordinary temperature in the presence of water to form compounds possessing cementitious properties [8,9]. The reaction is made possible through the dissolution of available and reactive species (especially silica and alumina) in the alkaline medium provided by calcium hydroxide. Most mineralogical phases are insoluble in water and unreactive even in the presence of dissolved calcium ions. However, their solubility is improved with increasing alkalinity, providing higher aqueous silicate and aluminate concentrations and enhanced reaction rates [5]. The reactivity of natural pozzolans is often assigned to glassy alumino-silicates [5,10]. However, due to alteration over time and natural hydration before extraction resulting in the formation of secondary minerals like clays or zeolites, the reactivity of pyroclastics is variable [5,11,12].

Natural pozzolans are not locally available in Northern France. However, a high volume of sediments is deposited on the seafloor of coastal ports and is dredged on a regular basis to avoid silting. Due to the saturation of storage spaces, the management of these marine sediments on land is increasingly difficult. Hence, there is a need to find new ways of reusing these materials in the building industry. Since marine sediments are partly derived from terrigenous sources (i.e. soil erosion) [13], a significant amount of quartz sand is commonly found in their mineralogical composition, along with feldspars and clay minerals [14]. Marine sediments may also contain calcium carbonate and organic matter. Literature is a bit controversial about the pozzolanic activity of quartz. However, several studies [15,16,17] agree on the need to make a mechanical activation of quartz powders to develop their reactivity. Strongly reducing the particle size increases the specific surface area, thus contributing to increase the surface free energy of particles due to the break of the chemical surface bonds [15]. According to Clerc [18], an ultra-fine grinding of particles will lead to the activation of their surface layers, resulting in a better dissolution of silica. Yao et al. [17] also found that prolonged grinding of quartz was beneficial to the decrease in the relative crystallinity and increase in the percentage of dissolution in an alkaline medium (provided by lime). In their paper, the grinding was done by means of a planetary ball mill during 160 minutes to reach a median diameter of 1.4 µm and a specific surface area (BET) of 5.5 $m^2.g^{-1}$. Following 60 days of moist curing at 20°C, a compressive strength of 14 MPa was reached for the paste sample designed with 80% of ground quartz and 20% of CaO. This strength performance appears to be high compared to the results of Wu et al. [15] who have investigated the effect of grinding intensity and specific surface area of quartz particles on the hydration activity at room temperature. The consumption of calcium hydroxide (CH) was found to increase with the specific surface area of quartz particles but the authors have reported a slow hardening kinetics for their blends (i.e. 80% of quartz mixed with 20% of CaO).

A compressive strength of 1.6 MPa was reached after 140 days for the highest specific surface area (730 $m^2.kg^{-1}$, Blaine). This shows that ground quartz has the capacity to react with CH at 20°C but the reaction kinetics is very slow and C-S-H are detected only after a long curing period [15]. Other authors [16] have defined a critical median diameter of 5 µm below which quartz particles possess strong pozzolanic reactivity at 100°C. Furthermore, some studies have revealed the benefit of mechanical grinding on the pozzolanic activity of feldspars (albite, microcline) and muscovite [19,20]. As regards the case of clay minerals, it is often reported that calcination is necessary for pozzolanic activation [5]. However, this treatment is energy consuming and the paper of Diamond et al. [21] showed that a mixture of lime and kaolinite (30 wt% of lime) had undergone cementation with a moist curing at 60°C. As a matter of fact, some materials with a high crystallinity can present an efficient pozzolanic behavior if the curing temperature is elevated. This was the case in a previous study dealing with pyroclastic materials and a quartz-rich sediment, both exhibiting a low amorphous content [22]. Hence, the ability of some minerals to combine a sufficient amount of lime has been shown to be highly dependent on the specific surface area of powders and the curing temperature of blends.

Some research is available about the reuse of calcined sediments as supplementary cementitious materials (SCMs) [23,24]. Nonetheless, in the present study, marine sediments from the port of Dunkirk (North of France) will be used without calcination but following micronization by air jet milling. Then, the sediments will be mixed with hydrated lime to produce a binder based on lime-pozzolan technology [25]. The first objective of the paper is to investigate the effect of the mineralogical composition of marine sediments for which the particle size distribution after micronization is the same (median diameter of about 2 µm) but the initial mass fractions of sand and fines are differently distributed. The question is to know if the results reported in a previous paper [22] could be extended to other mineralogical typologies. The second objective is to discuss the effect of the initial lime content introduced into the blend using three mix designs i.e. 10, 20 and 30 wt%. Based on literature on lime-pozzolan binders, the optimum lime content to achieve the best strength performances seem to be in the range of 15 to 30 wt% [6,7,10,26] but this will depend on the reaction kinetics and the nature of the alumino-silicate resource. Herein, the lime content will be studied with the sediment containing the highest amount of quartz. To keep the carbon footprint of the binder the lowest as possible, the lime content is limited to 30 wt.%. Conventionnaly, some reactivity tests (Chapelle, Frattini and strength activity index) have been used to differentiate reactive pozzolans from inert materials **[27]**. In more recent studies **[27,28]**, other methods working in SCM–CH systems in simulated cement pore solutions (R^3 tests) were found to be more relevant to predict the compressive strength development of cement mortars blended with SCMs. In the present study, lime (CH) is a reactant and part of the final binder. Thus the experimental methodology is based on the work of Pichon **[10]** where the pozzolanic reactivity is a function of lime combination (chemical term), newly-formed solid products and induced mechanical strength. Hence, the reactivity will be studied through the amount of fixed lime and bound water (reaction kinetics), the characterization of reaction products and the hardening kinetics at room (20°C) and elevated temperature (50°C). The paper will also go over the pore refinement at advanced curing ages (by MIP).

2. Materials and methods

2.1. Raw materials

Three different marine sediments (thereafter noted MS1, MS2 and MS3) were dredged in the port of Dunkirk (North of France) in 2019 and dehydrated by an active lagooning process. They can be all considered as non-hazardous and non-inert in compliance with the current regulation (99/31/EC). The fines contents was determined by wet sieving at 63 µm and was respectively estimated at 20, 40 and 70 wt% for MS1, MS2 and MS3 as seen in Fig. 1 in which the particle

size distribution of the sandy fraction (> 63 µm) performed by mechanical sieving is reported. The lime employed was a commercial high purity hydrated lime (SuperCalco®97 from Carmeuse). It was composed of 94 wt% of $Ca(OH)_2$ and 1.2 wt% of $CaCO_3$ (quantified by TGA).

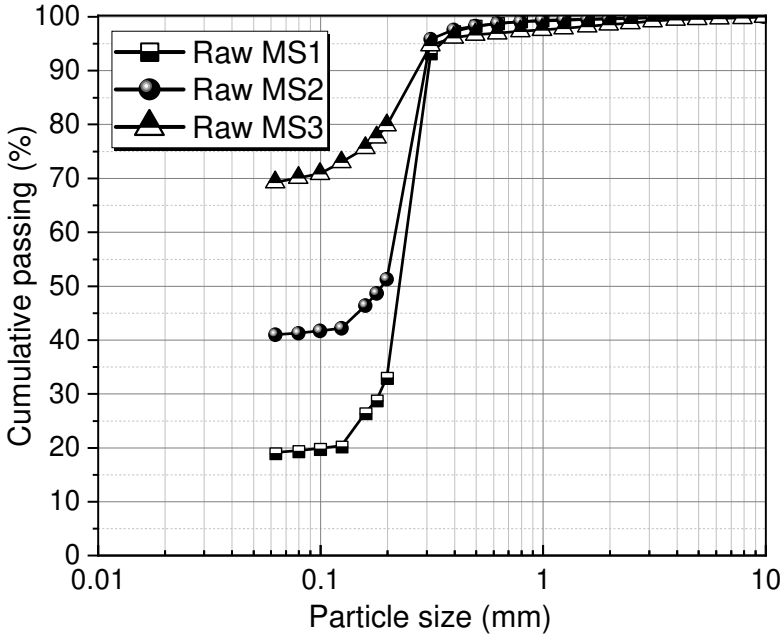

Fig. 1. Particle size distribution over 63 µm for the raw marine sediments

2.2. Experimental procedures

2.2.1. Micronization of sediments by air jet milling

After drying at 50°C, the sediments were ground to reach a maximum diameter of 500 µm using a Retsch rotor beater mill at a speed of 10,000 rpm. This input particle size was suitable before proceeding with the micronization by air jet milling. The equipment was set up to micronize the sediments to a median diameter (D_{50}) close to 2 µm [29]. A picture of micronized sediments is reported in Fig. 2.

2.2.2. Mix design and curing conditions

As a first step, the three micronized marine sediments were mixed with 20 wt% of hydrated lime to investigate the effect of their mineralogical composition on reaction and hardening kinetics. The mass ratio of lime to sediment was thereafter discussed working with MS2. The water-to-powder mass ratio (W/P) of the different blends depending on the physico-chemical properties of the sediments was determined by a flow spread test [30]. The mixtures were cast into cylindrical molds (2.7 cm in diameter and 5.4 cm in height) under the effect of vibration to avoid too much trapping of air bubbles. The molds were immediately introduced in airtight flasks to ensure endogenous conditions (RH > 95%) and avoid carbonation of hydrated lime. The samples were cured up to 365 days either at 20°C or 50°C.

2.2.3. Hardening and reaction kinetics

The compression tests were performed with a standard electromechanical press (Instron) equipped with a load cell whose capacity was 10 kN. The loading rate was 1.5 $kN.min^{-1}$. Compressive strength was measured from 3 to 365 days. For each testing age, the surface of samples was polished and the pastes were tested with the water saturation degree corresponding to the endogenous conditions.

For TGA, XRD and MIP after each curing age, a solvent exchange drying method with isopropyl alcohol (IPA) was used to remove capillary water. A representative sample of the cylinders was reduced to powder for TGA and XRD analyses and immersed in IPA for 7 days. The IPA was renewed twice (each time after 48 hours) to facilitate the exchange process. The IPA was then removed by vacuum drying and the samples were stored under vacuum in a desiccator with silica gel and hydrated lime until analysis to avoid carbonation as much as possible. The same protocol was followed to stop hydration on samples carefully cut out from the cylinders for MIP analysis. Thermogravimetric analysis (TGA) was performed with a Mettler Toledo instrument. Following hydration stoppage, the hardened samples were previously ground with a vibratory disc mill with a speed of 700 rpm for 1 min. The analysis was carried out under nitrogen atmosphere from 25°C to 950°C with a heating rate of 10°C.min^{-1}. Chemically bound water in hydrates was estimated from the mass loss in the range of 80°C to 400°C [31]. Free calcium hydroxide (CH) and calcium carbonate (CC) were quantified in the range of 400 to 500°C and 500 to 800°C respectively. The rate of CH combination depending on the kind of sediment used was calculated through the amount of fixed CH as percent of the initially available CH as follows: (Eq. (1))

$$\text{Fixed CH (\%)} = [(\text{CH}_i\ (\%) - \text{Free CH (\%)} - \text{Carbonated CH (\%)})/\text{CH}_i\ (\%)] \times 100 \quad (1)$$

Where CH_i (%) is the amount of CH initially introduced and carbonated CH (%) is the free lime that underwent carbonation, taking into account the initial content of CC in sediments.
For the reaction kinetics depending on the initial lime content, fixed CH was expressed in gram of CH per 100 grams of sediment (anhydrous powder) with MS (%), the initial weight percentage of marine sediment into the blend, following Eq. (2).

$$\text{Fixed CH (gCH/100g MS)} = [\text{CH}_i\ (\%) - \text{Free CH (\%)} - \text{Carbonated CH (\%)}] \times \frac{100}{\text{MS (\%)}} \quad (2)$$

XRD measurements were performed with Cu Kα radiation, 2θ from 10 to 80° and a step size of 0.02° (Bruker D2 phaser).
For porosity analysis, the samples were subjected to measurement after 90 and 180 days. The equipment was an AutoPore V 9600 Mercury porosimeter (from Micromeritics). The paste samples were inserted into a solids cell of volume 5 cm^3. The measurement was performed with pressure steps up to a maximum pressure of 200 MPa, corresponding to a minimum pore diameter of 6 nm. The total porosity (total volume of connected pores in the whole sample) and the differential intrusion distribution were provided. An examination of the pore size distribution was done through the critical pore diameter as described by Berodier et al. [32].

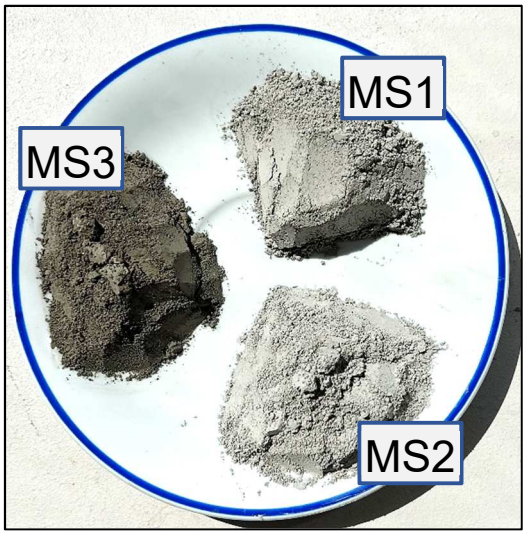

Fig. 2. Micronized powders of marine sediments

3. Results and discussion

3.1. Characterization of materials

The chemical compositions of micronized sediments determined by XRF are presented in Table 1. A variable amount of SiO_2 was highlighted i.e. 34, 58 and 73 wt% for MS3, MS1 and MS2 respectively. The high SiO_2 content of MS1 and MS2 is linked to the predominance of quartz sand, mainly contained in the fraction over 63 µm before micronization. Poor amounts of aluminum, iron and magnesium oxides were observed for these two sediments. Furthermore, from XRD patterns in Fig. 3, the mineralogical composition of MS1 and MS2 appears to be very similar with a strong presence of quartz and calcite. The presence of albite (feldspar, $NaAlSi_3O_8$), gypsum ($CaSO_4$, $2H_2O$) and pyrite (FeS_2) is also noted. However, MS3 stands out significantly from the other two sediments with a low SiO_2 content consistently with the high fines content before micronization (Fig. 1). This highlights the silty-clay nature of MS3 containing more aluminum-bearing minerals. Indeed, the presence of kaolinite (clay mineral, $Al_2Si_2O_5(OH)_4$) is clearly visible for MS3 whereas MS1 may contain a very low amount of this mineral (Fig. 3). With kaolinite, the strong presence of muscovite (potassium-rich mica that could also contain Fe, Mg and Mn) can be seen for MS3 along with the detection of microcline (feldspar, $KAlSi_3O_8$). The presence of these minerals explains the higher contents of Al_2O_3, Fe_2O_3 and K_2O of MS3 compared to MS1 and MS2. In addition, the X-ray diffraction peaks attributed to gypsum and pyrite in MS3 show higher intensities in compliance with higher amounts of Fe_2O_3 and SO_3.

Table 1. Chemical composition of marine sediments (previously calcined at 550°C) by XRF (in wt%)

Materials	SiO_2	Al_2O_3	Fe_2O_3	CaO	MgO	Na_2O	K_2O	TiO_2	P_2O_5	MnO	SO_3	LOI
MS1	57.9	3.5	2.0	8.9	0.6	1.2	1.0	0.1	0.1	–	1.2	22.9
MS2	73.4	3.0	1.9	8.3	0.5	1.0	0.9	0.1	0.1	–	1.1	9.3
MS3	34.4	9.7	7.7	19.6	2.4	1.3	1.9	0.4	0.4	0.2	3.8	17.7

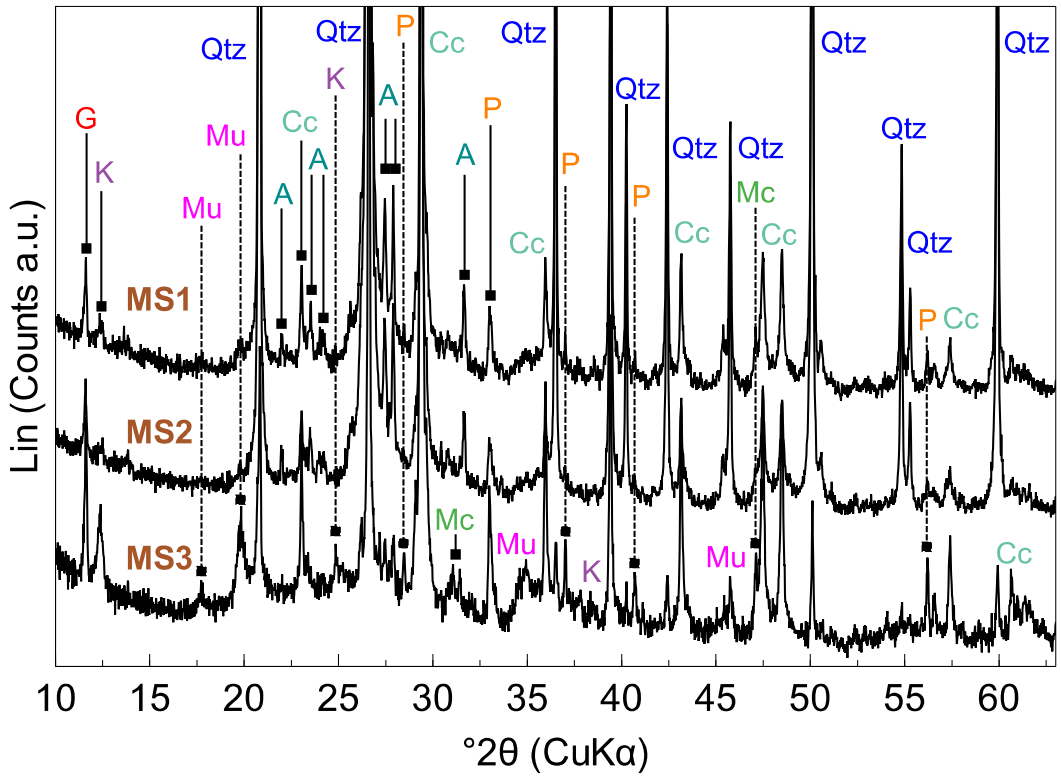

Fig. 3. XRD patterns of marine sediments. G: Gypsum, K: Kaolinite, Mu: Muscovite, Qtz: Quartz, A: Albite, Mc: Microcline, Cc: Calcite, P: Pyrite

The amounts of calcium carbonate (calcite) of sediments were quantified by TGA (500 ─ 800°C on DT─DTG curves reported in Fig. 4). This amount was found to be 38% for MS3 whereas it was 19─20% for MS1 and MS2. These results are in good agreement with the CaO contents reported in Table 1. Compared to MS1 and MS2, MS3 is relatively poor in quartz but calcite-rich. Following the elimination of physisorbed water, the mass loss around 120 ─ 125°C in TGA (Fig. 4) is attributed to the dehydration of gypsum to form anhydrite [33,34] confirming XRD results. According to Essaidi et al. [34], the slight mass loss around 480°C, especially visible on the DTG signal of MS3, is due to the structural dehydroxylation of kaolinite.

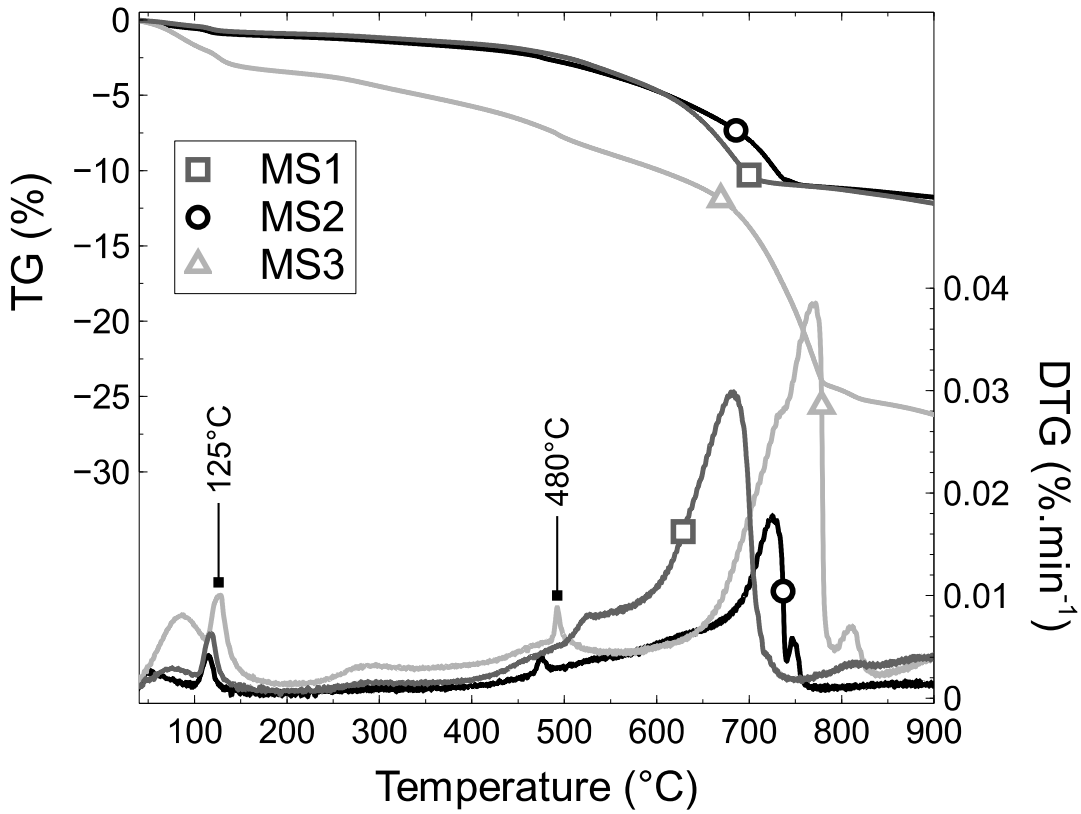

Fig. 4. TG-DTG curves of marine sediments

Following micronization, the particle size distribution of sediments is reported in Fig. 5 and compared to that of hydrated lime. It can be noted a very similar size range for the different sediment powders. Their median diameter is reported in Table 2 in which the physical properties are presented. The latter was in the range of 1.8 µm to 2.5 µm. Moreover, the maximum diameter was identical (about 7 µm). However, the BET specific surface area of MS3 was significantly higher than those reported for MS1 and MS2. This is explained by the different mineralogical composition of MS3 and could be linked to the higher LOI at 550°C measured for this sediment i.e. 16% versus 5 ─ 7% for the others (Table 2), partly reflecting the amount of organic matter. The latter, together with clay minerals, will tend to provide a much larger specific surface area for MS3.

Table 2. Physical properties of materials (micronized sediments and commercial hydrated lime)

Materials	MS1	MS2	MS3	Lime
Median diameter D_{50} (µm)	2.48	2.32	1.84	2.36
BET–SSA ($m^2.g^{-1}$)	6.90	4.54	18.91	17.66
True density ($g.cm^{-3}$)	2.64	2.65	2.47	2.33
LOI at 550°C (wt.%)	7.06	4.99	16.15	─

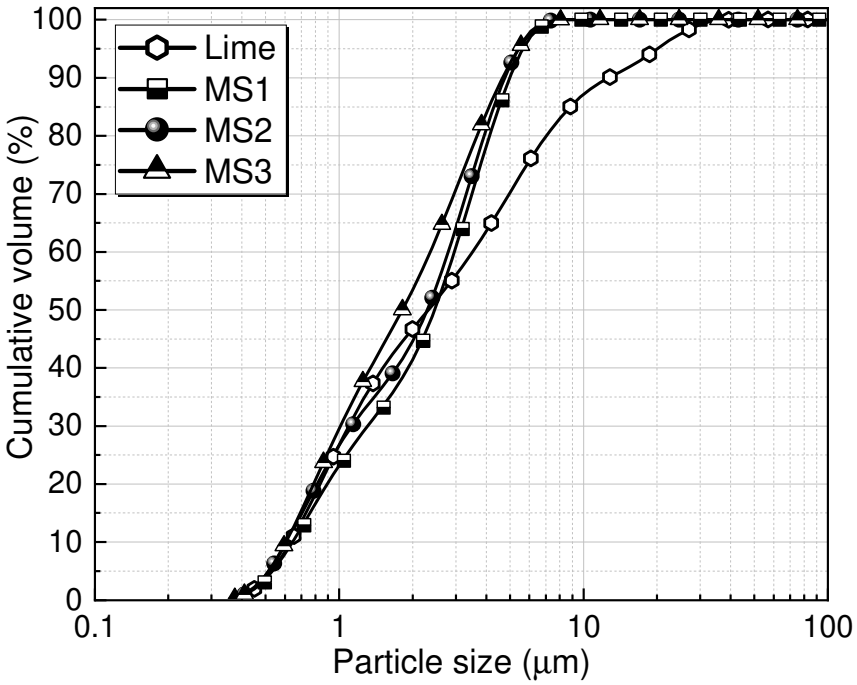

Fig. 5. Particle size distribution of sediment powders after micronization and hydrated lime

In connection with the physico-chemical properties of the sediments, the water-to-powder (W/P) mass ratio of lime-sediment pastes is reported in Table 3 (blends noted L20─MSn with n from 1 to 3 depending on the sediment used). The water demand was found to be higher for MS3 due to its high specific surface area. The W/P of Li─MS2 (with i = 10, 20 or 30 wt.% of lime) was kept constant (0.73).

Table 3. Water-to-powder ratios (W/P) of blends

Type of MS	MS (wt.%)	Lime (wt.%)	W/P	Designation
MS1	80	20	~~0.70~~ 0.80	L20─MS1
MS2	90/80/70	10/20/30	0.73	L10/20/30─MS2
MS3	80	20	1.10	L20─MS3

3.2. Compressive strength development

3.2.1. Ambient-cured samples

Firstly, it should be noted that none of the ambient-cured samples (20°C) were able to show a significant hardening before 90 days. At 365 days, the highest compressive strength was found to be 1.7 MPa for L20─MS2. This value is comparable to that measured by Wu et al. [15] on moist-cured pastes with 80 wt% of quartz and 20 wt% of lime at 140 days (1.6 MPa). The compressive strength of pastes including the other sediments (L20─MS1 and L20─MS3) was below 0.4 MPa even after a long curing time (one year). Furthermore, the effect of lime content was noticeable with lower performances for the mixes L10─MS2 and L30─MS2 (1.3 MPa and 0.9 MPa respectively after 365 days) compared to L20─MS2 (1.7 MPa).

3.2.2. Heat-cured samples

Fig. 6 presents the compressive strength development of blends cured at 50°C for 365 days and including 20 wt.% of lime depending on the type of sediment used. Until 180 days, the most significant strength development was found for L20─MS2. However, at 365 days, L20─MS1 finally reached a compressive strength of 12.3 MPa which was very close to that of L20─MS2 i.e. 13 MPa. The compressive strength of L20─MS3 was found to be significantly lower compared to

the other ones. In the latter case, the hardening only began from 60 days and the compressive strength at 365 days was 3.5 MPa. Even if the hardening kinetics was very slow, the elevated curing temperature was shown to be effective in increasing the compressive strength after a long curing period. At first sight, the different strength developments depending on the type of sediment can be attributed to the effect of various water-to-powder mass ratios, especially in the case of L20─MS3 for which an excess amount of water may lead to high porosity. However, it is noteworthy that the most significant hardening occurred by using the sediment for which the quartz content was the highest. According to literature dealing with quartz – CaO/CH – H_2O systems, intensive mechanical grinding and elevated curing temperature were found to increase the pozzolanic activity of quartz powders [16,17,35].

As a comparison, the strength development of blends designed with lime and ground basic pyroclastics (natural pozzolans) from a previous study [22] is also reported in Fig. 6 (grey area). The higher early age strength of lime–pozzolan binders is mainly due the lower water demand of pozzolans (W/P of mixes was about 0.4) compared to that of micronized sediments. However, except for L20─MS3, the compressive strength of lime–sediment binders exceeded that of lime–pozzolan binders (12─13 MPa versus 8 MPa at the most after 365 days) despite the higher W/P (0.7─0.8). This highlights the positive effect of the micronized quartz-rich sediments on the strength development in the long run.

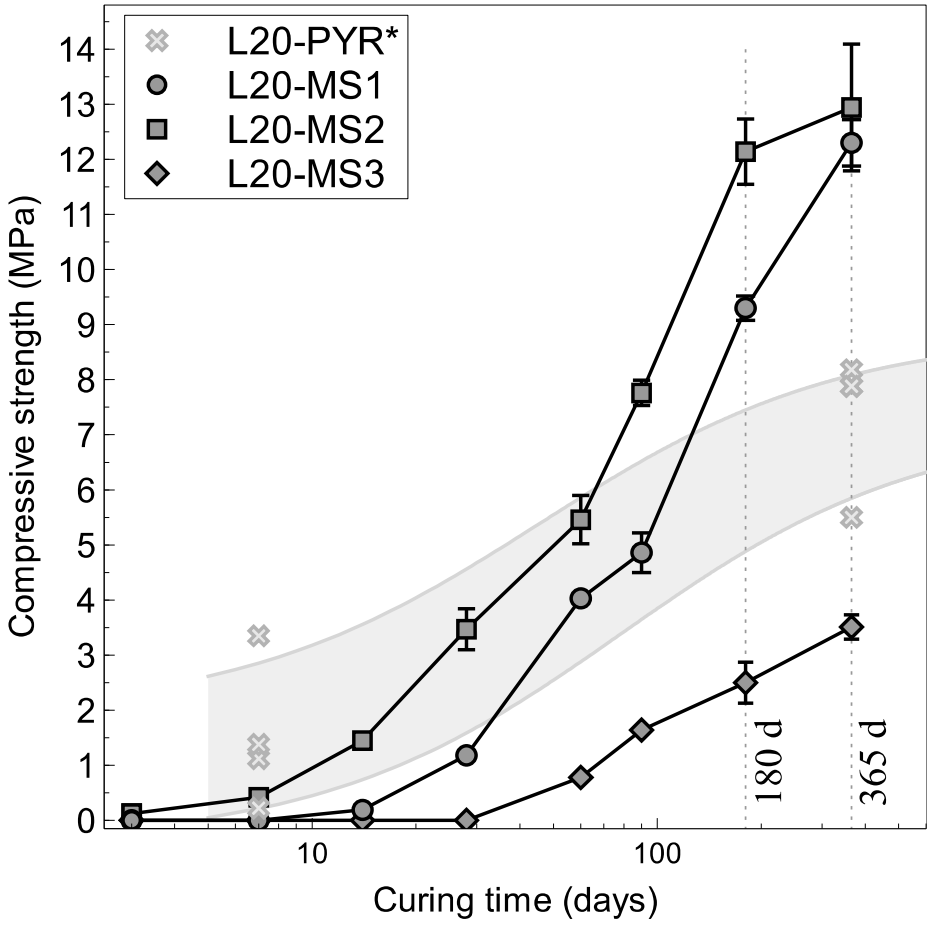

Fig. 6. Compressive strength development of L20─MSn at 50°C depending on the type of marine sediment used. *L20─PYR = lime-pyroclastics binders from Kourtaa et al. [22]

The effect of lime content on the strength development of Li─MS2 is reported in Fig. 7. The compressive strength of L30─MS2 was found to be lower compared to that of L20─MS2 until 180 days. However, the compressive strength of L30─MS2 showed a significant increase from 180 to 365 days in such a way that the compressive at 365 days was the same (13 MPa). With

regard to L10—MS2, the trend was to level off from 60 days and the increase in compressive strength from 60 days to 365 days was very low (5 to 5.8 MPa). In their study about CaO-quartz blends with 5 to 20 wt% of CaO, Yao et al. [17] measured the highest compressive strength at 28 days for the blend with 10 wt.% of CaO whereas the optimum compressive strength at 60 days was reported for 20 wt.% of CaO (14 MPa). Even if the curing temperature was not the same, this trend shows similarities with the present study where the compressive strength of L10—MS2 was of the same order or even higher than that of L30—MS2 from early age to 60 days whereas the compressive strength of L30—MS2 in the long term was significantly higher compared to that of L10—MS2. The study of hydration kinetics will provide a better understanding of these results. However, these results show that it is not necessary to include more than 20 wt.% of lime in the mix to improve the strength during the first weeks. As a matter of fact, the heat curing process will have to be time-limited for industrial application and energy efficiency.

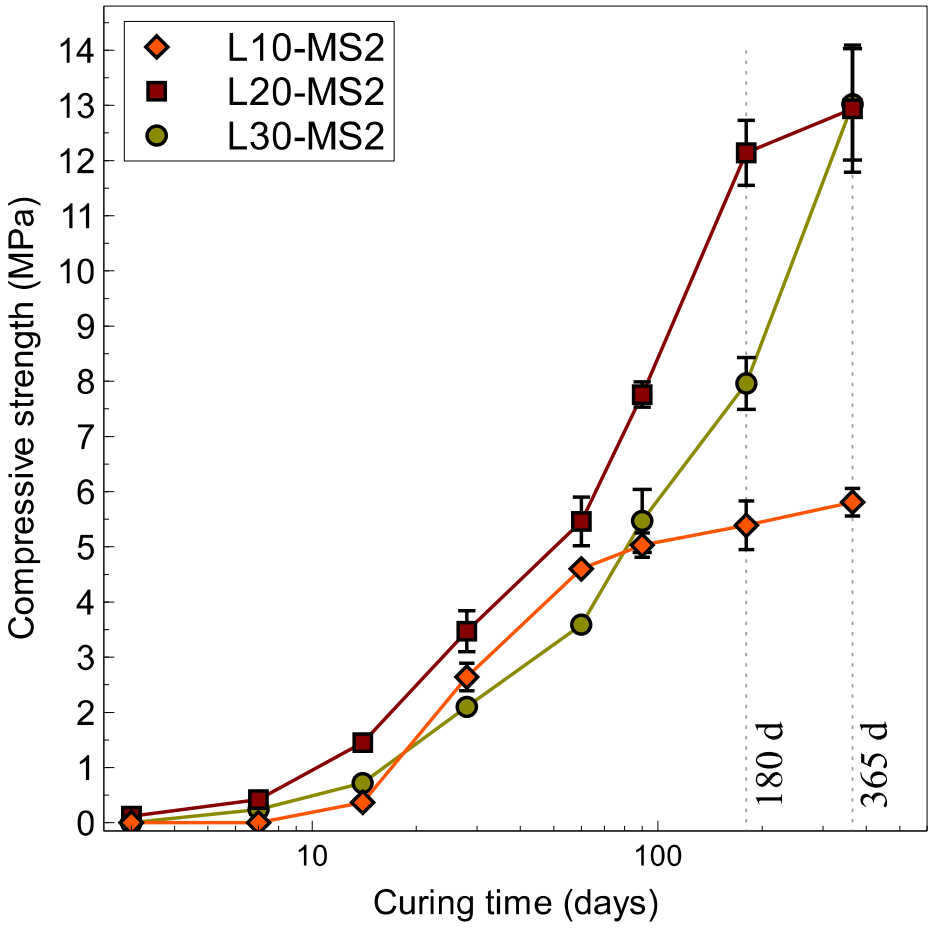

Fig. 7. Compressive strength development of Li—MS2 at 50°C (i = 10, 20 or 30 wt.% of lime)

3.3. Hydration kinetics

3.3.1. Fixed lime

The amount of fixed CH over time as percent of the initially available CH depending on the type of sediment used is reported in Fig. 8. At 20 °C (Fig. 8a), CH was consumed quickly during the first week, up to around 25—30%. At 50 °C (Fig. 8b), the amount of fixed CH after 7 days was not much higher than that calculated at 20°C i.e. in the range of 35—40%. However, the rate of CH combination beyond this date was very different depending on the curing temperature. At 20 °C, the combination rate was slow from 7 to 60 days and the amount of fixed CH tended to level off from 60 to 365 days. After 365 days, this amount was in the range of 45—55%. On the contrary, a

significant increase in the rate of CH combination was observed from 7 to 60 days at 50°C. Moreover, the whole combination of CH was achieved between 60 and 180 days depending on the sediment used. This finding applies to all sediments and is explained by an increase in soluble silica with temperature. According to some authors, the pozzolanic reaction occurs initially at edge surfaces of quartz (or clay minerals) by CH attack [21,36]. At room temperature, the slow rate of quartz dissolution is assumed to result in a progressive reduction in CH combination as seen in Fig. 8a whereas elevated temperature provides higher amounts of reactive species allowing the reaction to proceed until the full depletion of CH (Fig. 8b). At this stage, the poor hardening of blends at 20°C even after several months (1.7 MPa at the most after 1 year) can be attributed to an insufficient amount of combined lime together with the nature of C─S─H formed at this temperature (Ca/Si, gel pores, etc.).

Furthermore, at 20°C, the combination of CH was found to be more significant in the case of L20─MS3 with more than 50% of CH already reacted with MS3 at 60 days whereas this amount was 30─35% with the other two sediments. This result is attributed to the huge specific surface area of MS3 (~19 $m^2.g^{-1}$) increasing the rate of CH chemisorption [37]. At 50°C, this effect of specific surface area was not perceivable. This shows that the rate of CH combination at 20°C (and the short-term activity at 50°C) strongly depends on the specific surface area of powders whereas the full depletion of CH is possible through elevated temperature (50°C) and rather related to the mineralogical composition of the sediments. Therefore, an accelerated reaction kinetics was found for the blends including the sediments containing higher quartz contents i.e. MS1 and MS2 (Fig. 8b). The low amount of silica within MS3 (34%) did not prevent it to fix the whole content of initially available lime after 180 days. Hence, the total silica content is not a limiting factor for CH combination. Nevertheless, quartz is not the only mineral able to bind lime. For MS3, some aluminum-bearing minerals such as kaolinite, feldspars and muscovite could contribute to the consumption of CH.

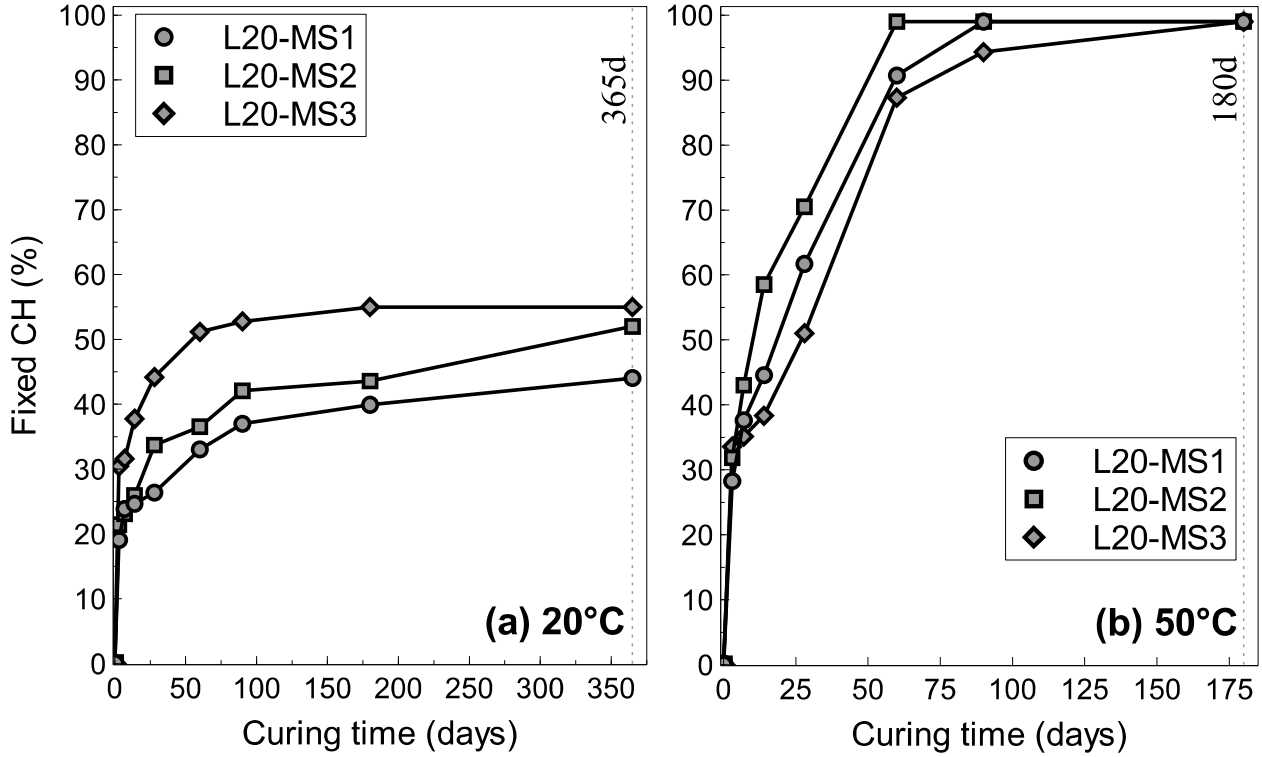

Fig. 8. Fixed lime depending on the type of marine sediment used (L20─MSn)

Fig. 9a presents the combination of CH by MS2 at 20°C depending on the initial content of lime expressed in gram of CH per 100 grams of sediment from 3 to 365 days.

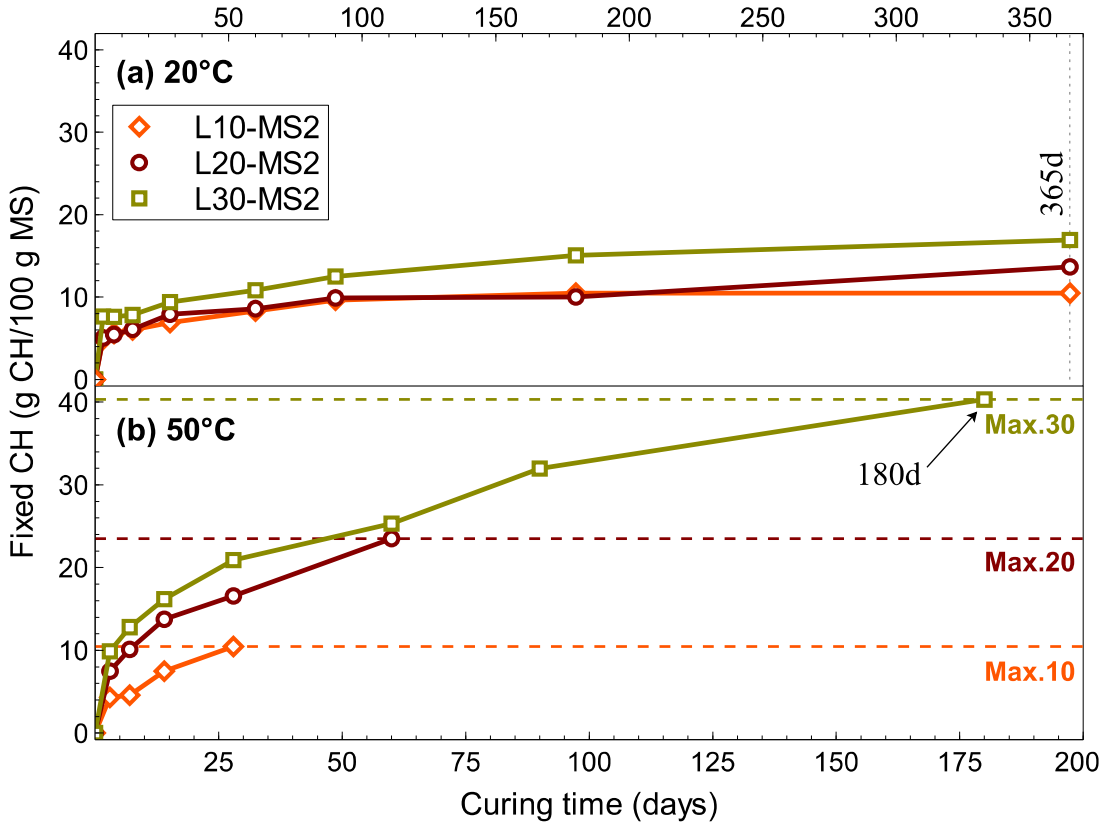

Fig. 9. Fixed lime by MS2 over time depending on the initial lime content (Li─MS2) **(a)** 20°C, **(b)** 50°C

The rate of CH combination was quite similar for L10─MS2 and L20─MS2 and somewhat higher for L30─MS2. After 365 days, the absolute amount of fixed CH was in the range of 10.5 ─ 17 grams of CH per 100 grams of sediment depending on the initial amount of lime introduced. It is interesting to note that the sediment was able to fix all the lime in the case of L10─MS2 and around half of the initially available lime in the case of L20─MS2, corresponding to a close absolute amount of fixed CH. This confirms a slowdown of the chemical reaction at 20°C. Even if a little more CH was combined in the case of L30─MS2, a levelling off was also clearly observed over time.

The reaction kinetics at 50°C is reported in Fig. 9b. Up to 28 days, it can be seen that more CH was consumed per gram of starting sediment per unit time when the initial amount of lime into the blend was higher. However, the more was the initial amount of lime, the longer it took to reach the full depletion of CH. The latter was achieved after 28 days for L10─MS2, 60 days for L20─MS2 and 180 days for L30─MS2. As regards L10─MS2, the stabilization of the compressive strength beyond 60 days is consistent with the lack of lime in the reaction system. Furthermore, it should be recalled that the compressive strength after 365 days at 50°C was 5.8 MPa whereas that at 20°C was only 1.3 MPa even though the amount of fixed CH was the same (10.5 grams of CH per 100 grams of sediment). Based on the assumption that the amount of soluble silica is higher at 50°C, this result is explained by a lower Ca/Si ratio of C─S─H at 50°C compared to 20°C as suggested by Arabi et al. [38]. It is known that the strength contribution of C─S─H increases with the decrease in the Ca/Si ratio [38,39,40]. This discussion done in the case of L10─MS2 underlines the significant role of the C─S─H microstructure on the strength development compared to the absolute amount of fixed CH. An increase in this amount is only of interest at 50°C and allows for a greater strength in the long run (5.8 MPa for L30─MS2 compared to 13 MPa for L20─MS2 at 365 days).

By comparing L20─MS2 and L30─MS2, the lower compressive strength of L30─MS2 up to 180 days is ascribed to the higher amount of unreacted lime. According to Jambor [41], uncombined

CH in lime-pozzolan binders has the same unfavourable influence on strength as porosity. However, this excess CH was beneficial for the further strength development at 365 days as also observed by Yao et al. [17] with CaO-quartz blends. In a previous investigation **[22]**, SEM analysis had shown that the reaction at the microstructural scale proceeds as if lime was gradually converted in hydration products in which some embedded lime nodules took a long time to be combined.

3.3.2. Bound water and reaction products

TG–DTG data from the analysis of samples with 20 wt% of lime cured at 20°C or 50°C depending on the sediment used are reported in Fig. 10.

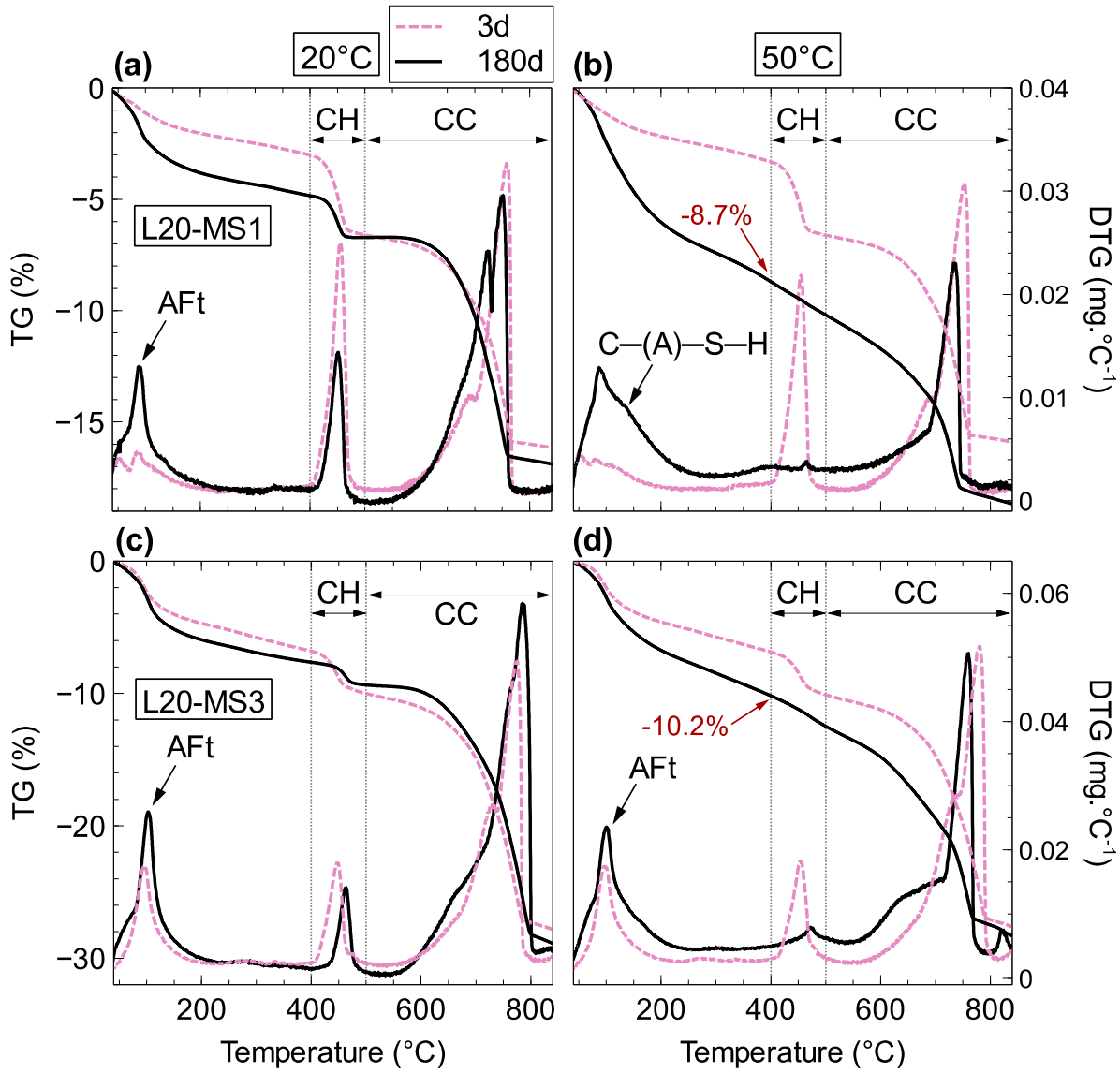

Fig. 10. TG-DTG curves of samples cured for 3 days or 180 days. **(a)** L20–MS1 at 20°C, **(b)** L20–MS1 at 50°C, **(c)** L20–MS3 at 20°C, **(d)** L20–MS3 at 50°C

It should be noted that signals recorded for L20–MS1 and L20–MS2 were very close together and, as a consequence, only that of L20–MS1 is reported in Fig. 10. An advanced curing time (180 days) is compared to the early age (3 days). At 20°C and for the early age at 50°C, the amount of CC was found to be rather high considering the initial amount of CC within the sediments. However, after CH depletion at 50°C, the amount of CC in hydrated samples became

very close to the initial amount within the sediments following the normalization to anhydrous powder since chemically bound water in hydration products increases with time. This shows that the carbonation of CH (see Eq. (1)) likely occurred during the preparation of the samples before analysis despite the precautions taken.

Studying the binders cured for 180 days at 50°C, the weight losses at 400°C by TGA are indicated in Fig. 10b and d. These have to be corrected by removing physisorbed water before 80°C and initial weight loss attributed to the dehydration of the anhydrous sediment powder (Fig. 4) to estimate the bound water in hydrates. This amount was found to be in the range of 5.8 – 6.4% for L20–MS1 and L20–MS2 whereas a somewhat lower amount was calculated for L20–MS3 (~5%). After 365 days, this amount of bound water was found to be the same irrespective of the sediment used, in the range of 5.9 – 6.5%. However, the compressive strength of L20–MS3 was significantly lower compared to the binders using the other two sediments, partially indicating a different phase assemblage of hydrated binders.

XRD patterns of binders cured 180 days are presented in Fig. 11 and compared to those of the micronized sediments. As in the case of TGA, L20–MS1 and L20–MS2 are characterized by a same pattern and only that of L20–MS2 is reported.

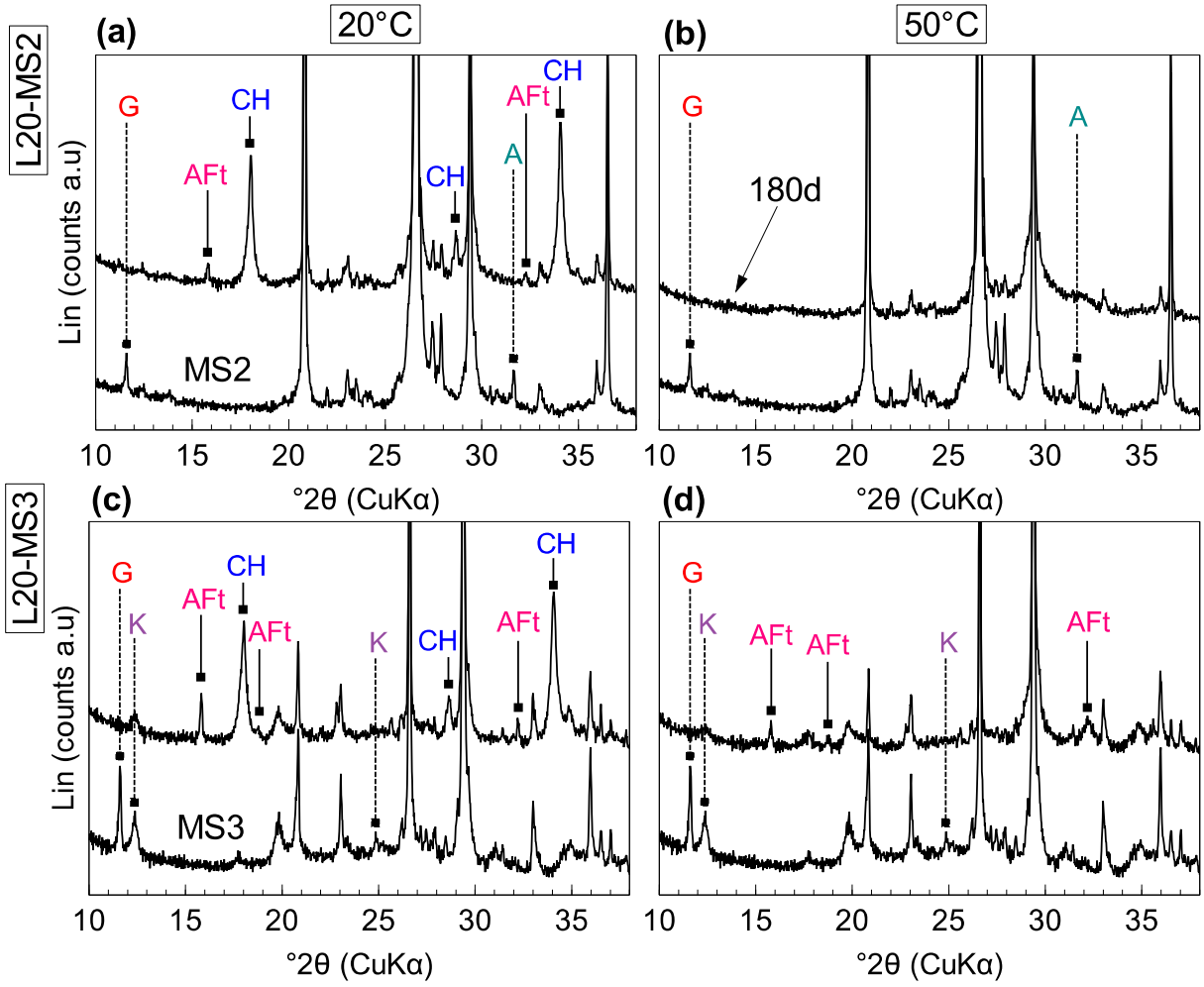

Fig. 11. XRD patterns at 180 days of **(a)** L20–MS2 at 20°C, **(b)** L20–MS2 at 50°C, **(c)** L20–MS3 at 20°C, **(d)** L20–MS3 at 50°C. MS2 & MS3: XRD patterns of sediments. G: Gypsum, AFt: Ettringite, CH: Calcium Hydroxide, A: Albite (feldspar), K: Kaolinite

For both curing temperatures, it can be seen that gypsum was fully consumed. In addition, it is shown that feldspars (for L20─MS1 and L20─MS2) and kaolinite (for L20─MS3) were involved in the pozzolanic reaction. However, no changes were observed regarding the diffraction peaks of muscovite in L20─MS3. At the same time, the only hydration product clearly detected by XRD was AFt (ettringite, $C_6As_3H_{32}$) and the latter was quickly formed. This is attributed to the dissolution of aluminum-bearing minerals and releasing of $[H_3AlO_4]^{2-}$, which upon reaction with Ca^{2+}, SO_4^{2-} and OH^- from lime and gypsum will lead to the formation of AFt [19]. However, at 50°C, AFt was progressively destabilized from 3 to 28 days and was no longer detected for L20─MS1 and L20─MS2 at advanced curing ages (Fig. 11b) whereas it was still present for L20─MS3 even after 180 days (Fig. 11d). This is explained by the higher amounts of aqueous aluminate and sulfate concentrations in the medium in the case of L20─MS3. Hence, gypsum and kaolinite within MS3 are strongly involved in the significant formation of AFt. On the contrary, the sulfate deficient medium for L20─MS1 and L20─MS2 is likely to be responsible for the destabilization of AFt initially present in lower amounts. The disappearance of AFt in Fig. 11b was not accompanied by the visible presence of AFm by XRD analysis. However, according to the work of Zhou and Glasser [42] about the thermal stability and the decomposition mechanisms of AFt, a temperature exceeding 50°C may lead to a decrease in crystallinity, and consequently, to the gradual disappearance of the diffraction peak [43].

Considering the derivative weight loss, the range between 80°C and 400°C includes weight losses due to the dehydration of AFt and C–(A)–S–H phases but the latter could not be identified by XRD due to the overlapping with calcite and their low crystallinity. Combining DTG data with XRD results, it is assumed that the weight loss peak around 80 ─ 100°C at 20°C (Fig. 10a and c) is mainly attributed to the decomposition of AFt. At 50°C, the more extended mass loss (broader DTG peak up to 250 ─ 300°C) is considered as the dehydration of C─(A)─S─H. This is especially the case for L20─MS1 (Fig. 10b) thus highlighting the lower amount of C─(A)─S─H for L20─MS3 compared to L20─MS1 and L20─MS2. Hence, the similar amount of bound water in hydrates calculated for the three blends after 365 days at 50°C (~6%) can be explained by the larger amount of AFt in L20─MS3 since this is a water-rich phase [44] (576 $g.mol^{-1}$ of H_2O loss compared to 27 ─ 36 $g.mol^{-1}$ for C─S─H according to Lothenbach et al. [33]). Either way, from the overall results, the contribution of AFt to the strength appears to be minor in the systems studied in this paper whereas it is known for efficiently filling the pores [45].

TGA and XRD patterns depending on the initial lime content (Li ─ MS2) have shown the same trend. For these blends, Fig. 12 reports the evolution of bound water in hydrates over time (from 3 to 365 days) at 50°C and a comparison with the strength development. Firstly, it is observed that the amount of bound water at a given hydration time increased with the initial lime content as also found in the works of Yao et al. [17,20] mixing quartz or feldspars with increasing amounts of CaO (5 ─ 30 wt.%). Furthermore, the compressive strength of L20─MS2 rose faster than that of L30─MS2 until 180 days whereas the bound water content of L30─MS2 was almost still higher for the different curing times. This highlights the different degree of reaction at a given curing time depending on the lime content. For instance, at 28 days, the degree of reaction of L20─MS2 was 0.7 whereas it was 0.5 for L30─MS2. Hence, the higher amount of uncombined lime, which itself leads to the formation of high-Ca C─S─H, adversely affects the compressive strength of L30─MS2. Over time, more reactive species dissolve into the pore solution even after CH depletion, giving rise to low-Ca C─S─H [34,46]. This happened earlier for L20─MS2 and results in a smaller increase in the bound water content between 60 and 365 days compared to L30─MS2. It should also be noted that the stabilization of compressive strength of L10─MS2 beyond 60 days is consistent with the bound water content that levels off as of 28 days.

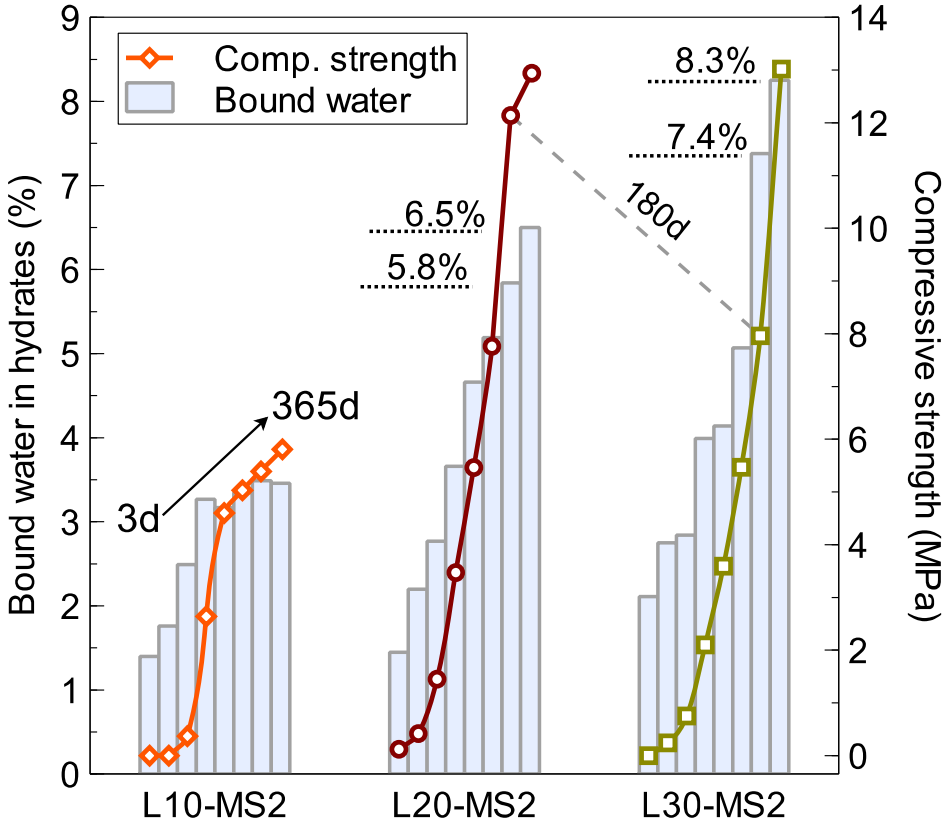

Fig. 12. Bound water in hydrates from 3 to 365 days of curing at 50 °C depending on the lime content and comparison with the strength development

3.4. Porosity

Table 4 shows the total porosities of the different L─MS binders. Depending on the amount of hydrated lime initially introduced, the total porosity after 180 days at 50°C ranged between 55 and 59 vol.% for L20─MS1 and L20─MS2 whereas it was around 68 vol.% for L20─MS3. As a matter of fact, the total porosity of L20─MS3 was found to be significantly higher compared to that of L20─MS1 and L20─MS2 owing to the high W/P mass ratio used for this blend (1.10 versus 0.73 ─ 0.80 ~~0.73~~ for the other ones). The total pore volume does not necessarily correlate with compressive strength results since the latter is mainly dependent on the nature and the packing of hydration products. For instance, the same total porosity after 180 days at 50°C for L20─MS2 and L30─MS2 (~55 vol%) corresponds to different compressive strengths i.e. 12.1 MPa for L20─MS2 versus 8 MPa for L30─MS2. For a better analysis of the pore network, the pore size distribution needs to be discussed.

Table 4. Total porosities (expressed in vol%)

L – MS binders		L20─MSn			Li─MS2	
Curing T°C	Curing time	L20─MS1	L20–MS2	L20–MS3	L10–MS2	L30–MS2
20°C	90d	61.7	57.8	66.7	60.6	60.8
	180d	63.6	57.0	66.6	60.7	60.1
50°C	90d	60.6	58.4	67.5	58.4	57.4
	180d	59.1	55.4	67.7	57.9	55.2

The effect of curing temperature on the pore size distribution of the different blends depending on the sediment used is reported in Fig. 13a and b for 90 days and the critical pore diameter is provided for 90 and 180 days in Fig. 13c.

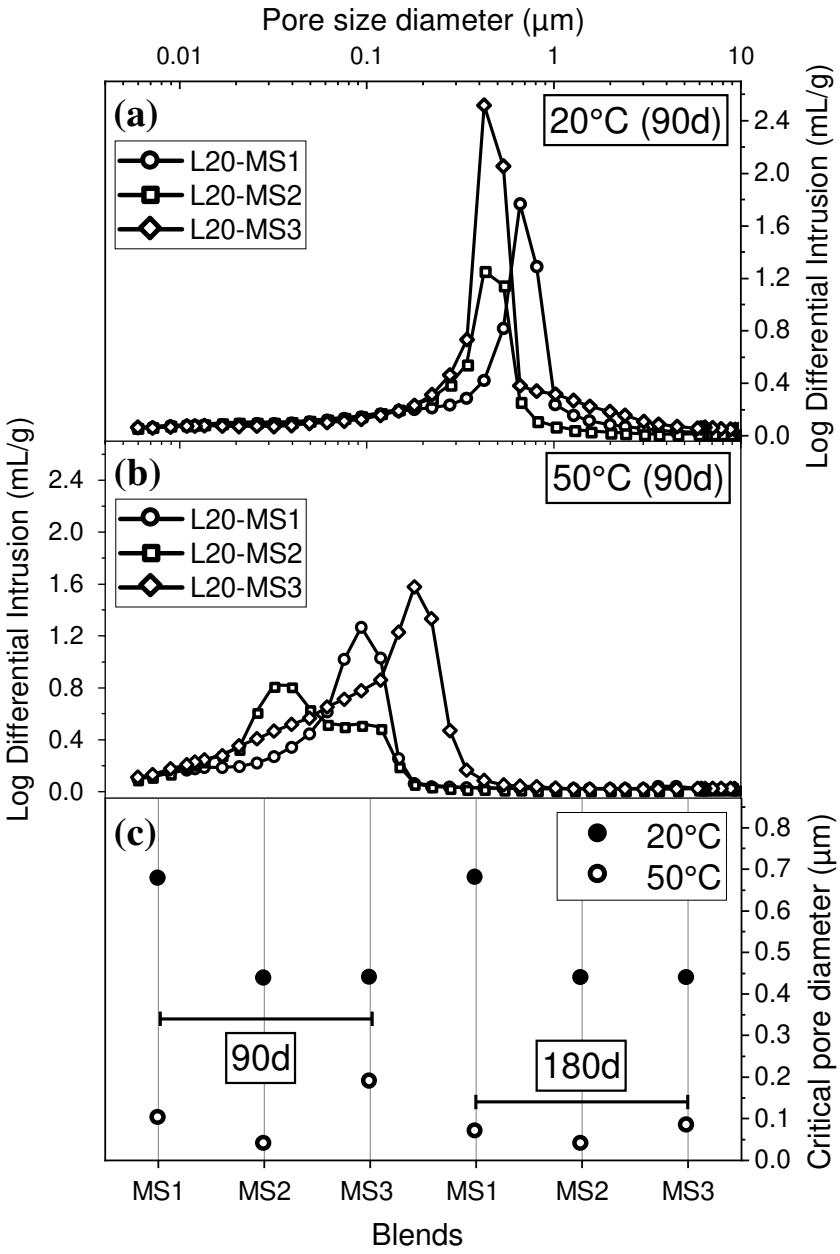

Fig. 13. Differential distribution of mercury intrusion depending on the sediment used (L20─MSn) and the curing temperature **(a)** 20°C, **(b)** 50°C, **(c)** critical pore diameter (MSn for L20─MSn on the x-axis)

As a first observation, a significant pore size refinement was noted by comparing the blends at 20°C and 50°C after 90 days due to the partial filling of the pores by hydration products (Fig. 13a and b). At 20°C, the critical pore diameter of the blends was over 0.2 µm corresponding to coarse pores that are reported to be harmful for the strength [47]. Hence, AFt formation at 20°C that should be responsible for filling the pores does not provide a significant strength since none of the ambient-cured samples were able to show hardening before 90 days. It is also noted that no changes were noted between 90 and 180 days regarding the critical pore diameter at 20°C (Fig. 13c) and this may be linked to lime combination that levels off as seen in Fig. 8a. The pore size refinement at 50°C results in the reduction of the critical pore diameter as seen in Fig. 13c. The critical pore diameters of the different blends were in good agreement with the compressive strength at this date with increasing critical pore diameters (0.03 µm, 0.1 µm and 0.18 µm for MS1, MS2 and MS3) corresponding to a decreasing strength (respectively 7.8 MPa, 4.9 MPa and 1.6 MPa). In addition, it should be noted that the pore size refinement between 20°C and 50°C for

L20─MS3 at 90 days was lower compared to the other ones. However, after 180 days, the critical pore diameter of L20─MS3 at 50°C has moved closer to that of L20─MS1 with a critical pore diameter of 0.08 µm for L20─MS3 and 0.06 µm for L20─MS1 (Fig. 13c). The pore size refinement between 90 days and 180 days at 50°C is therefore clearly observed for both L20─MS1 and L20─MS3. Despite this decrease in the critical pore diameter, the compressive strength of L20─MS3 remains very low compared to L20─MS1 owing to the high total pore volume as shown in Table 4. In the case of L20─MS2 for which the porosity already showed a strong filling of pores by hydration products after 90 days at 50°C, the critical pore diameter after 180 days remained unchanged compared to 90 days (0.03 µm). Yet, a significant strength development was noted between 90 and 180 days. This is explained by the pore size distribution of this blend for which the pore family around 0.08 ─ 0.1 µm observed at 90 days (Fig. 13b and Fig. 14a) was no longer present at 180 days as shown in Fig. 14b. This is not reflected by the critical pore diameter but through the median pore diameter as shown in a previous study [22].

Considering the effect of lime content, since the W/P was identical for all the mixes, it is possible to compare the total porosities in Table 4 without considering the capillary pores due to excess water. However, these total pore volumes were close together i.e. in the order of ± 3 vol% for each curing temperature. Here again, it is more relevant to discuss the differential pore size distribution depending on the lime content (Li─MS2) as reported in Fig. 14a and b for heat-cured samples after 90 and 180 days. At 90 days, the critical pore diameters of Li─MS2 are consistent with their compressive strength. The critical pore diameter of L10─MS2 was fairly close to that of L30─MS2 (in the range of 0.08 to 0.12 µm) and the compressive strength of both blends was in the range of 5 ─ 5.5 MPa. However, L20─MS2 stood out from the other ones with a critical pore diameter of 0.03 µm and a compressive strength of 7.8 MPa. After 180 days, a significant pore size refinement of L30─MS2 was measured, identified by the dotted line in Fig. 14a and b. The critical pore diameter has moved closer to that of L20─MS2 (0.04 µm versus 0.03 µm). This is in accordance with the strength development of L30─MS2 after advanced curing ages and the compressive strength achieved at 365 days which is finally the same as that of L20─MS2 (13 MPa). Moreover, the overall results presented in Fig. 14c show that the best pore size refinement after 90 and 180 days was always found for L20─MS2 whichever the curing temperature, confirming the compressive strength results.

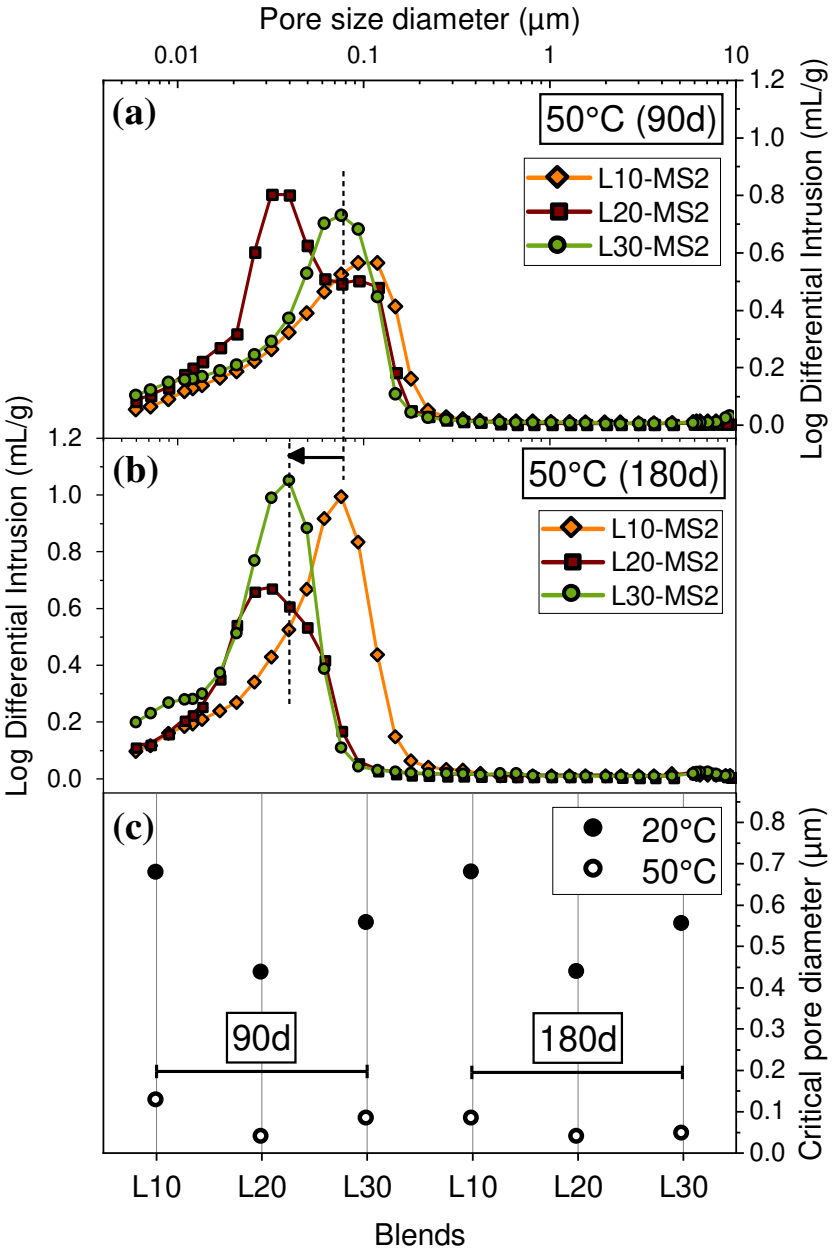

Fig. 14. Differential distribution of mercury intrusion depending on the lime content (Li─MS2) at 50°C **(a)** 90 days, **(b)** 180 days **(c)** critical pore diameter (Li for Li─MS2 on the x-axis)

4. Conclusion

The following conclusions can be made :

(1) The best hardening kinetics of heat-cured lime-sediment blends was found with the sediment for which the quartz content was the highest (~70 wt% SiO_2). Thus, the full depletion of calcium hydroxide was achieved after 180 days when the lime content was 30 wt% (corresponding to 40 grams of CH per 100 grams of sediment). Despite the effectiveness of micronization and heat curing (50°C) to increase the dissolution of reactive species in such a way to reach high amounts of fixed lime, the pozzolanic reaction was found to take a long time. However, the results are quite in line with previous works dealing with quartz-lime-water systems.

(2) At 20°C, none of the three sediments studied were able to combine more than about 15 grams of CH per 100 grams of sediment (i.e. half of the initially available lime when the lime content was 20 wt%), even with the sediment exhibiting the highest specific surface area (~19 $m^2.g^{-1}$). However, at 50°C and in the case of 20 wt% of lime into the blends, all the sediments were able to reach the full depletion of CH from 60 to 180 days, whichever their SiO_2 content.

(3) One of the sediment (MS3) was poor in quartz (~34 wt% SiO_2) but contained higher amounts of aluminum- and sulfate/sulfur- bearing minerals (i.e. kaolinite, muscovite, gypsum and pyrite). This led to the more significant persistence of AFt at 50°C until at least 180 days. However, TGA results suggest that the amount of C─(A)─S─H was lower using this sediment compared to the other ones containing higher SiO_2 contents (58 – 73%). In addition, the lime–MS3 binder was affected by a higher total porosity due to high water content for the mixing. Furthermore, the formation of AFt at 20°C is not enough to provide a measurable strength at 20°C and this may be due to the insufficient filling of coarse pores whereas C─(A)─S─H can strongly contribute to the cementation, especially at 50°C.

(4) Until 180 days, the optimum compressive strength was achieved for 20 wt% of lime for both curing temperatures. At 50°C, blends with 10 wt% of lime suffered from a lack of lime as of 60 days. Those with 30 wt% of lime needed more time to reach a sufficient consumption of CH and finally filled the gap with the blends containing 20 wt% of lime at 365 days (compressive strength of 13 MPa).

(5) Studying the effect of lime content with a same water content, a strong correlation between the critical pore diameter and the compressive strength was highlighted.

Acknowledgments

The authors would like to thank the Hauts-de-France region and the European Regional Development Fund (ERDF) for financial support.
They are also grateful to G. Potier (MIP & technical support), M. D'Helft (technical support), P. Bedart (strength test & technical support) and Y. Zaleski (TGA).

Highlights

- Hydration of lime-marine sediment blends depending on the mineralogical composition
- Cristallized minerals in micronized sediments can efficiently combine hydrated lime
- Full depletion of CH with 20 wt% of lime regardless of the silica content
- Contribution of AFt to the strength is negligible beside total pore volume in samples
- For a same W/P, the critical pore diameter strongly correlates with the strength

References

[1] M. Chabannes, F. Becquart, N.-E. Abriak. Shear strength of unbound crop by-products using the direct shear box apparatus. Journal of Renewable Materials, 7(9), 2019, 855-863.
[2] J.H. Arehart, W.S. Nelson, W. V. Srubar. On the theoretical carbon storage and carbon sequestration potential of hempcrete. Journal of Cleaner Production 266, 2020, 121846.
[3] A. Arrigoni, R. Pelosato, P. Melia, G. Ruggieri, S. Sabbadini, G. Dotelli. Life cycle assessment of natural building materials: the role of carbonation, mixture components and transport in the environmental impacts of hempcrete blocks, Journal of Cleaner Production 149, 2017, 1051-1061.
[4] S. Pretot, F. Collet, C. Garnier. Life cycle assessment of a hemp concrete wall: impact of thickness and coating. Building and Environment 72, 2014, 223-213.

606 [5] E. M. Gartner, D. E. Macphee. A physico-chemical basis for novel cementitious binders.
607 Cement and Concrete Research 41, 2011, 736-749.
608 [6] C. Shi, R. L. Day. Comparison of different methods for enhancing reactivity of pozzolans.
609 Cement and Concrete Research 31(5), 2001, 813-818.
610 [7] V. Nozahic, S. Amziane, G. Torrent, K. Saïdi, H. De Baynast. Design of green concrete made
611 of plant-derived aggregates and a pumice-lime binder. Cement and Concrete Composites 34,
612 2012, 231-241.
613 [8] S. Donatello, M. Tyrer, C.R. Cheeseman. Comparison of test methods to assess pozzolanic
614 activity. Cement and Concrete Composites 32, 2010, 121-127.
615 [9] American Society for Testing and Materials (ASTM) C125. Standard terminology relating to
616 concrete and concrete aggregates, 2007.
617 [10] H. Pichon. Le système « pouzzolanes naturelles – chaux – eau » à 38°C et 100°C : relations
618 entre la réactivité chimique, les phases néoformées et les conséquences physico-mécaniques
619 (application aux matériaux volcaniques du Massif Central français), PhD Thesis, Université
620 Joseph Fourier, 1994, p. 234.
621 [11] A. Maropoulou, B. Bakolas, E. Aggelakopoulou. Evaluation of pozzolanic activity of natural
622 and artifical pozzolans by thermal analysis. Thermochimica Acta 420, 2004, 135-140.
623 [12] G. Habert, H. Choupay, J.M. Montel, D. Guillaume, G. Escadeillas. Effects of the secondary
624 minerals of the natural pozzolans on their pozzolanic activity. Cement and Concrete Research 38-
625 7, 2008, 963-975.
626 [13] Y. Mamindy-Pajany, C. Hurel, F. Geret, M. Romeo, N. Marmier. Comparison of mineral-
627 based amendments for ex-situ stabilization of trace elements (As, Cd, Cu, Mo, Ni, Zn) in marine
628 dredged sediments: A pilote scale experiment. Journal of Hazardous Materials 252-253, 2013,
629 213-219.
630 [14] Y.-H. Li, J. E. Schoonmaker. Chemical composition and mineralogy of marine sediments.
631 Treatise on Geochemistry, vol.7, ISBN 0-08-043751-6. Elsevier, p 1-35.
632 [15] P. Wu, X. Lyu, J. Wang, S. Hu. Effect of mechanical grinding on the hydration activity of
633 quartz in the presence of calcium hydroxide. Advances in Cement Research 29 (7), 2017, 269-
634 277.
635 [16] J.-C. Bénézet, A. Benhassaine. Grinding and pozzolanic reactivity of quartz powders. Powder
636 Technology 105, 1999, 167-171.
637 [17] G. Yao, T. Cui, J. Zhang, J. Wang, X. Lyu. Effects of mechanical grinding on pozzolanic
638 activity and hydration properties of quartz. Advanced Powder Technology 31 (11), 2020, 4500-
639 4509.
640 [18] L. Clerc. Broyage ultrafin de carbonates naturels : Paramétrisation, modélisation et
641 conséquences physico-chimiques, PhD Thesis, Ecole Nationale Supérieure des Mines de St-
642 Etienne et Institut National Polytechnique de Grenoble, 1992, p. 170.
643 [19] G. Yao, Q. Liu, J. Wang, P. Wu, X. Lyu. Effect of mechanical grinding on pozzolanic
644 activity and hydration properties of siliceous gold ore tailings. Journal of Cleaner Production 217,
645 2019, 12-21.
646 [20] G. Yao, Z. Wang, J. Xao, X. Cong, C. Anning, X. Lyu. Pozzolanic activity and hydration
647 properties of feldspar after mechanical activation. Powder Technology 383, 2021, 167-174.
648 [21] S. Diamond. Transformation of clay minerals by calcium hydroxide attack. Clay and Clay
649 Minerals, 12 (1), 1963, 359-379.
650 [22] S. Kourtaa, M. Chabannes, F. Becquart, N.-E. Abriak. Evaluation of marine dredged
651 sediment as reactive powder compared to ground basaltic pyroclastic materials for the
652 development of eco-friendly lime-pozzolan binders. Cement and Concrete Composites 130, 2022,
653 104553.
654 [23] R. Snellings, O. Cizer, L. Horckmans, P.T. Durdzinski, P. Dierckx, P. Nielsen, K. Van Balen,
655 L. Vanderwelle. Properties and pozzolanic reactivity of flash calcined dredging sediments.
656 Applied Clay Science 129, 2016, 35-39.

[24] J. Skibsted, R. Snellings. Reactivity of supplementary cementitious materials (SCMs) in cement blends. Cement and Concrete Research 124, 2019, 105799.
[25] H. Goldsworthy, Z. Min. Mortar studies towards the replication of Roman Concrete. Archaeometry 51 (6), 2009, 932-946.
[26] C. Shi, R. L. Day. Chemical activation of blended cements made with lime and natural pozzolans. Cement and Concrete Research 23 (6), 1993, 1389-1396.
[27] S. Ramanathan, M. Kasaniya, M. Tuen, M.D.A. Thomas, P. Suraneni. Linking reactivity tests outputs to properties of cementitious pastes made with supplementary cementitious materials. Cement and Concrete Composites 114, 2020, 103742.
[28] Development of a new rapid, relevant and reliable (R^3) test method to evaluate the pozzolanic reactivity of calcined kaolinitic clays. Cement and Concrete Research 85, 2016, 1-11.
[29] T. Lacombe. Formulation et solidification par voie hydrothermale de charges minérales poreuses à base cimentaire : application aux matières premières secondaires, cas des sédiments de dragage portuaire. PhD Thesis of Lille University, 2020.
[30] P. Domone, C. His-Wen. Testing binders for high-performance concrete. Cement and Concrete Research, 27(8), 1997, 1141-1147.
[31] A. Bakolas, E. Aggelakopoulou. Pozzolanic activity of natural pozzolan-lime pastes and physico-chemical characteristics. Journal of Thermal Analysis and Calorimetry 135, 2019, 2953-2961.
[32] E. Berodier, J. Bizzozero, A.C.A. Muller. Mercury intrusion porosimetry, in K.L. Scrivener, R. Snellings, B. Lothenbach (Eds.), A practical guide to microstructural analysis of cementitious materials, CRC Press Taylor & Francis Group, Boca Raton, 2016, pp. 419-444.
[33] B. Lothenbach, P. Durdzinski, K. De Weerdt. Thermogravimetric analysis, in: K.L. Scrivener, R. Snellings, B. Lothenbach (Eds.), A practical guide to microstructural analysis of Cementitious Materials, CRC Press Taylor and Francis Group, Boca Raton, 2016, pp. 419-444
[34] N. Essaidi, B. Samet, S. Baklouti, S. Rossignol. Fesability of producing geopolymers from two different Tunisian clays before and after calcination at various temperatures. Applied Clay Science 88-89, 2014, 221-227.
[35] S-H. Kang, H. Kang, N. Lee, Y-H. Kwon. Utilization of lime-based alternative hydration to develop cementless UHPFRC. Journal of Building Engineering 45 (2022) 103668.
[36] E.R. Cook, B. Batchelor, Chapter 4. Stabilization/solidification of hazardous wastes in soil matrices, In : Y. Corapcioglu (Eds.), Advances in Porous Media, 3, 1996, 307-359.
[37] S.A. Greenberg. Reaction between silica and calcium hydroxide solutions. I. Kinetics in the temperature range 30 to 85°C. Journal of Physical Chemistry, 1961, 65, 1, 12-16.
[38] N. Arabi, R. Jauberthie, N. Chelghoum, L. Molez. Formation of C-S-H in calcium hydroxide-blast furnace slag-quartz-water system in autoclaving conditions. Advances in Cement Research, 2015, 27(3), 153-162.
[39] W. Kunter, S. Ferreiro, J. Skibsted. Influence of the Ca/Si ratio on the compressive strength of cementitious calcium-silicate-hydrate binders. Journal of Materials Chemistry A, 2017, 5, 17401.
[40] J. Wang, Z. Hu, Y. Chen, J. Huang, Y. Ma, W. Zhu, J. Liu. Effect of Ca/Si and Al/Si on micromechanical properties of C-(A)-S-H. Cement and Concrete Research 157, 2022, 106811.
[41] J. Jambor. Relation between phase composition, over-all porosiy and strength of hardened lime-pozzolana pastes, Magazine of Concrete Research, 1963, No. 45.
[42] Q. Zhou, F.P. Glasser. Thermal stability and decomposition of mechanisms of ettringite at <120°C. Cement and Concrete Research 31, 2001, 1333-1339.
[43] Y. Wan, Y. Chen, B. Guo, S. Zhang, Y. Tong, D. Niu. Study on the strength and hydration behavior of sulfate-resistant cement in high geothermal environment. Materials, 2022, 15, 2790.
[44] G. Le Saout, B. Lothenbach, P. Taquet, H. Fryda, F. Winnefeld. Hydration of calcium aluminate cement blended with anhydrite. Advances in Cement Research, Thomas Teldord, 2018, 30 (1), pp. 24-36.

708 [45] G. Yao, T. Cui, Z. Jia, S. Sun, C. Anning, J. Qiu, X. Lyu. Effect of anhydrite on hydration
709 properties of mechanically activated muscovite in the presence of calcium oxide. Applied Clay
710 Science, 196, 2020, 105742.
711 [46] H. Maraghechi, M. Maraghechi, F. Rajabipour, C.G. Pantano. Pozzolanic reactivity of
712 recycled glass powder at elevated temperatures: Reaction stoichiometry, reaction products and
713 effect of alkali activation. Cement and Concrete Composites 53, 2014, 105-114.
714 [47] S. Cheng, Z. Shui, T. Sun, R. Yu, G. Zhang. Durability and microstructure of coral sand
715 concrete incorporating supplementary cementitious materials. Construction and Building
716 Materials 171 (2018), 44-53.